This is a peer-reviewed, accepted author manuscript of the following research article: Zhao, W, Liu, J, Li, T, Song, H, Chen, B, Chen, B & Li, G 2025, 'Contrasting effects of temperature rise in different seasons on larger and smaller phytoplankton assemblages in a temperate coastal water, Laoshan Bay, northern Yellow Sea, China', *Marine Environmental Research*, vol. 206, 107034. https://doi.org/10.1016/j.marenvres.2025.107034

Contrasting effects of temperature rise in different seasons on larger and smaller phytoplankton assemblages in a temperate coastal water, Laoshan Bay, northern Yellow Sea, China

Wei Zhao[1,3], Jihua Liu[1,3,4]*, Tingting Li[5], Hui Song[1,3], Bokun Chen[3], Bingzhang Chen[6], Gang Li[2]*

[1]Institute of Marine Science and Technology, Shandong University, Qingdao 266237, China

[2]Daya Bay Marine Biology Research Station & Key Laboratory of Tropical Marine Bio-Resources and Ecology, South China Sea Institute of Oceanology, Chinese Academy of Sciences, Guangzhou 510530, China

[3]Joint Laboratory for Ocean Research and Education of Dalhousie University, Shandong University and Xiamen University, Qingdao 266237, China

[4]Qingdao Key Laboratory of Ocean Carbon Sequestration and Negative Emission Technology, Shandong University, Qingdao 266237, China

[5]School of Life Sciences, Qufu Normal University, Qufu, 273165, China

[6]Department of Mathematics and Statistics, University of Strathclyde, Glasgow G1 1XH, UK

* Correspondence: Jihua Liu, liujihua1982@foxmail.com; Gang Li, ligang@scsio.ac.cn

Abstract: Anthropogenic influences and climate change are leading to more frequent and intense heatwaves, which are known to affect marine ecosystems. However, the effects of rising temperatures on *in-situ* phytoplankton size classes have not yet been adequately studied. In this study, two cell-sized phytoplankton assemblages (>20 μm, <20 μm) were cultured at a range of temperatures [i.e., ambient temperature (AT), AT+3 ºC, AT+6 ºC and AT+9 ºC] in Laoshan Bay, Yellow Sea, China, at half-month intervals between June 2022 and July 2023. Total chlorophyll *a* concentration fluctuated between 0.84 and 7.76 μg L^{-1} throughout the year, with the highest value presented in winter with the lowest proportion of smaller cells. Photosynthetic efficiency (F_V/F_M) of larger cells, which varied between 0.15 in winter and 0.52 in summer, was 22% higher than their smaller counterparts, while their growth rate (μ, -0.21 to 0.91 d^{-1}) was 60% higher. The slope derived from the linear fit of F_V/F_M or μ to temperature, an indicator of temperature sensitivity, was positive in winter but negative in summer, depending mainly on ambient temperature. The μ of larger cells was increased more than that of smaller cells by an increase in temperature in winter, but inhibited more in summer, indicating their greater sensitivity to temperature. Our results also showed that the integrated inhibition of a 1 ºC temperature increase over one year is 5.45% and 3.68% on the growth of larger and smaller cells, respectively, suggesting a negative effect of temperature increase on phytoplankton community in Laoshan Bay.

Keywords: Temperature rise, Fluorescence, Growth, Seasonal variation, Phytoplankton assemblages, Laoshan Bay

1. Introduction

As a result of anthropogenic activities and climate change, the intensity and frequency of oceanic extreme weather events, marine heatwaves (MHWs), are increasing, with temperatures rising by up to 8-9 ºC within a short period of time and their annual duration increasing to over 110 days (Frölicher and Laufkötter 2018; Yao et al. 2020). Such an increase in temperature affects many physiological processes of marine phytoplankton such as photosynthesis, the synthesis of proteins and lipids (Flanjak et al. 2022), the efficiency of ion transport (Jabre et al. 2020) and enzymatic activities (Zuccarini et al. 2020), altering their growth and biomass and ultimately affecting the marine biogeochemical cycle and ecosystem functioning (Sepúlveda and Cantarero 2022).

Previous studies have shown that the effects of rising temperatures on the biochemistry and physiology of phytoplankton vary greatly depending on the specific species and ambient temperature. For example, an increase in temperature stimulated the growth of the diatoms *Pseudo-nitzschia* and *Skeletonema dohrnii*, accompanied by the upregulated light harvesting complexes proteins and enhanced nitrogen assimilation processes (Jabre et al. 2020; Cheng et al. 2022). The increase in temperature also improved the photosynthetic carbon assimilation efficiency of the diatom *Phaeodactylum tricornutum* and chlorophyta *Chlorella vulgaris* by promoting the consumption of excess reducing energy to stabilize the plastid ATP: NADPH ratio, and further allocate more photosynthate for growth by down-regulating respiration (Padfield et al. 2015; Rehder et al. 2023). However, the

insignificant and even negative effects of temperature rise have also been observed on the growth of the diatom *Fragilariopsis* and prymnesiophyceae *Phaeocystis antarctica* (Jabre et al. 2020; Aflenzer et al. 2023). Regarding natural phytoplankton assemblages, Mai et al. (2021) and Dalpadado et al. (2023) also reported a negative effect of rising temperatures on their photosynthesis in tropical oceans, while Jabre et al. (2020) found an increasing trend in nutrient uptake and primary productivity in the Southern Ocean. All these results suggest that the effects of rising temperatures on phytoplankton may not be uniform. Whether and to what extent such effects depend on ambient temperatures and species differences is still unclear.

It is generally assumed that rising temperatures will lead to a miniaturization of phytoplankton communities, possibly due to reduced dissolved O_2, increased CO_2 or the blocking of nutrient upshift from the deep layers as the sea surface warms (Finkel et al. 2010; Liu et al. 2023). As one of the most important factors regulating marine primary productivity, phytoplankton cell size often varies greatly in nature, with species-specific sizes spanning more than nine orders of magnitude in volume, from the smallest cyanobacteria at less than 1.0 μm^3 to the largest diatoms at over 10^8 μm^3 (Finkel et al. 2010). Cell size often regulates the physiological responses of phytoplankton to environmental changes (Schulhof et al. 2019). Compared to larger cells, smaller phytoplankton cells are more efficient at absorbing nutrients due to their higher surface area-to-volume ratio (Clark et al. 2013), so they are likely to be more competitive when nutrients are scarce due to

temperature rise. A case study in the western North Pacific confirmed the miniaturization, and showed a positive correlation between the growth rate of piconano-phytoplankton assemblages and temperature but an insignificant correlation in micro-assemblages (Liu et al. 2022), although it did not rule out the influence of other physico-chemical factors. In addition, an increase in temperature caused a more positive regulation of cell pigments and photosynthetic activity in smaller diatom *Thalassiosira pseudonana*, but not in larger *T. punctigera* (Xu et al. 2020), which only reflects the individual responses. The direct effects of an increase in temperature on *in-situ* phytoplankton assemblages with different cell sizes need to be studied.

In the present study, we examined the effects of rising temperatures on larger and smaller phytoplankton assemblages at different times of the year to determine: (1) how phytoplankton community structure changes seasonally; (2) how rising temperatures affect the photosynthetic physiology and growth of phytoplankton assemblages at different background temperatures, and (3) how different the responses, i.e. temperature sensitivity, of larger and smaller phytoplankton to rising temperatures are and how they change over the course of a year. To assess the effects of rising temperatures, we measured the growth and photophysiology of larger (>20 μm) and smaller phytoplankton assemblages (<20 μm) from a temperate coastal area, Laoshan Bay, at a range of temperatures [i.e., ambient (AT), AT+3 ºC, AT+6 ºC and AT+9 ºC] in a half-month interval from June 2022 to July 2023. To our knowledge, this is the first time that the effects of rising temperatures on *in situ*

phytoplankton assemblages have been investigated in a year-round study.

2. Materials and Methods

2.1. Study area and sampling protocol

This study was carried out with phytoplankton assemblages collected at sea surface (~0.50 m) in Laoshan Bay (120º43'E, 36º21'N), northern Yellow Sea, China (Fig. 1). The Laoshan Bay is geographically located in the northern Yellow Sea, China (Fig. 1), with annual temperature fluctuations between 4.57 and 29.48 °C (Liu et al. 2016). This bay is a semi-enclosed bay with irregular semi-diurnal tides and covers an area of ~188 km^2 with a maximum depth of 14 m (Sun et al. 2016). Fish farming has been introduced in Laoshan Bay since the 1980s, and today it is an important ecological farming area where fish, shrimp, clams, sea cucumbers, abalone, among others, are farmed, and has become one of the most developed continental shelf areas in the world (Dong et al. 2023). Apart from a high population of fish and benthic animals, a rich biodiversity has also been reported in this bay (Su et al. 2022). In recent years, rapid warming has been observed in this area (Wang et al. 2023).

The laboratory cultivation was conducted 500 m off the sampling site at the Institute of Marine Science and Technology, Shandong University, Qingdao City, Shandong Province, China. There are studies report that result from laboratory experiment is consistent with *in situ* observation data (Daufresne et al. 2009), as well as articles studying the effect of

environmental change on in situ photosynthetic assemblages based on laboratory experiment (Jabre et.al 2020; Liu et.al 2022). During experimentation, surface seawater was taken with a 25 L acid-cleaned (1 N HCl) polycarbonate carboy during spring tide and returned to laboratory (15 min away from the sampling site) where experiments were performed as described below. The study site was visited every two weeks from June 26, 2022 (Julian Day 177) to July 30, 2023 (next Julian Day 211).

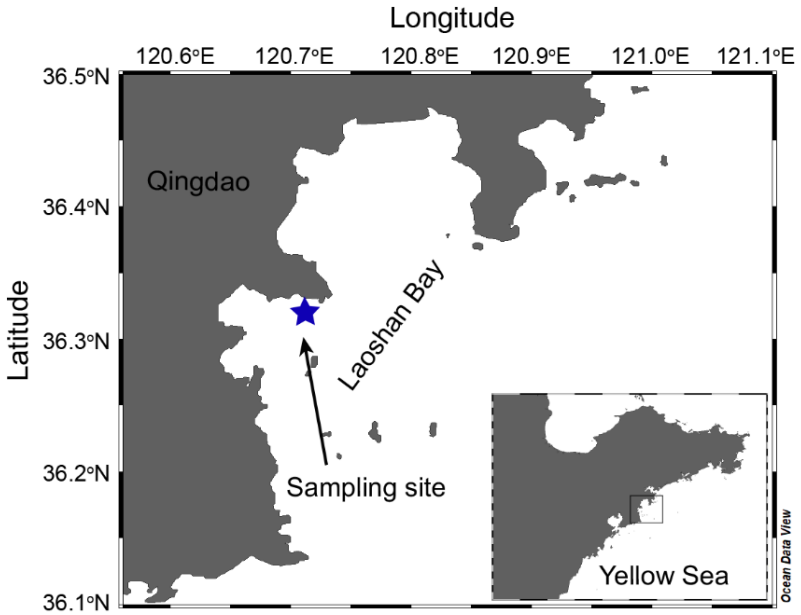

Fig. 1. Map of Laoshan Bay in the Yellow Sea, China, with a star indicating the sampling site.

2.2. Experimental design

In the laboratory, the collected seawater was pre-filtered through a 200 μm pore-sized mesh to eliminate the effect of mesozooplankton and then filtered sequentially onto a 20 μm pore-sized PC membrane (47 mm in diameter, Millipore) and a 0.2 μm pore-sized PC

membrane (47 mm, Millipore). Phytoplankton retained on the filters were gently resuspended in 3.5 L of 0.2 μm filtered *in situ* seawater collected at each sampling time-point. To eliminate the interference of filtration with physiology, every 500 mL of natural seawater was filtered with one filter. The concentrated larger (>20 μm) and smaller phytoplankton assemblages (<20 μm) were then adjusted to approximately field conditions and dispensed in 1-liter flasks.

To evaluate the effects of temperature rise, the flasks were maintained at four temperature conditions, i.e. ambient temperature (AT), AT+3, AT+6 and AT+9 ºC, in a plant growth chamber (Zhichu, Shanghai, China) for 24 hours, in which the four temperatures changed over the time of sampling. According to RCP 8.5 scenario (IPCC 2013), sea surface temperatures would rise by 4 ºC by the end of 2100, while the temperatures rise could reach up to 9 ºC in short period due to marine heatwaves (Frolicher and Laufkotter 2018). We therefore set a maximum increase of 9 ºC in this study. During the short-term (24 h) incubation, we did not detect the distinct variations of nutrients contents. The light in the chamber was set to 150 μmol photons m^{-2} s^{-1}, with a Light:Dark cycle of 12:12. This light intensity corresponds to about 50% of upper euphotic zone in the northern Yellow Sea (Bai et al. 2005). We used 3 replicates for each treatment and a total of 24 flasks at each experiment. Before and after the 24-hour incubation, samples were taken from each flask to measure chlorophyll fluorescence and concentration as follows.

2.3. Chlorophyll fluorescence measurements

Before and after incubation, aliquots of 10 mL sample were taken from each of the four temperature-treated flasks and dark-acclimated for 15 min to oxidize electron transport chains and relax non-photochemical quenching in the chamber of the Fast Repetition Rate Fluorometer (FRRf) coupled to a FastAct base unit (Fast Ocean, Chelsea Technologies Group, Ltd., West Molesey, UK) (Schuback et al. 2021). The FRRf was then activated with a single turnover protocol consisting of 100 saturation flashets of 1-μs duration with 2-μs pitch, followed by 40 relaxation flashets with 60-μs pitch (Kolber et al. 1998). For each measurement, there was a series of 10 actinic light exposures that varied from 0 to 2000 μmol photons m^{-2} s^{-1} and lasted 60 s each. The actinic light was provided by a blue excitation LED (450 nm) in the FastAct device. There was a 20-s dark interval between each light exposure step, and the first light step lasted 120 s because phytoplankton require more time to acclimate to the initial transition from the dark to the illuminated state (Wei et al. 2019). The fluorescence yield from each step was recorded and averaged from 30 consecutive recordings. The minimum and maximum fluorescence yields in the dark (F_O, F_M) and light-regulated states (F', F'_M) were derived from the curve of the fluorescence transient according to Kolber et al. (1998). In addition, chlorophyll fluorescence was adjusted by subtracting the fluorescence of 0.2 μm pore-sized PC membrane-filtered seawater to eliminate the influence of background fluorescence (Cullen and Davis 2003). The photochemical quantum yields (F_V/F_M, F_q/F'_M) of photosystem II (PS II) in the dark

and light states were calculated according to Genty et al. (1989):

$$F_V/F_M=(F_M-F_O)/F_M;\ F_q/F'_M=(F'_M-F')/F'_M \quad (1)$$

The rapid light response curve (RLC)-derived light utilization efficiency (α) and saturation irradiance (E_K, μmol photons m^{-2} s^{-1}) were calculated according to Silsbe and Kromkamp (2012):

$$F_q/F'_M=\alpha\times E_K\times(1-e^{-E/E_K})\times E^{-1} \quad (2)$$

where E indicates the actinic light intensity (μmol photons m^{-2} s^{-1}).

The maximal electron transfer rate (ETR_{max}) was calculated as follows:

$$ETR_{max}=\alpha\times E_K \quad (3)$$

2.4. Growth rate measurements

To measure the growth of phytoplankton, Chl *a* biomass in each flask of the four temperature treatments was measured as described below and the specific growth rate (μ, d^{-1}) was estimated as:

$$\mu=\frac{\ln(N_t)-\ln(N_0)}{t-t_0} \quad (4)$$

where N_t and N_0 indicate Chl *a* concentration at time t_0 and t, respectively.

To quantify Chl *a* concentration, 100 mL cultures of larger or smaller cells were filtered onto PC filters (25 mm diameter) with 0.2 μm pore size and extracted overnight with 5 mL magnesium carbonate ($MgCO_3$)-saturated 90% acetone (v/v) at 4 ºC in the dark. After centrifugation at 4 ºC (4000 rpm) for 10 min, the optical absorbance of the supernatant was measured from 400 to 750 nm using a scanning spectrophotometer (Shimadzu model UV

1800-PC, Kyoto, Japan). The Chl *a* concentration was calculated according to Porra (2004):

$$\text{Chl } a = 11.47\times(A_{664}-A_{750})-0.4\times(A_{630}-A_{750}) \quad (5)$$

where A_{630}, A_{664}, and A_{750} indicate the absorbance at 640 nm, 664 nm, and 750 nm, respectively.

2.5. Temperature sensitivity

To estimate the effects of an increase in temperature, photosynthetic efficiency (F_V/F_M) and growth rate (μ) of larger and smaller phytoplankton assemblages were plotted against temperature. The slopes (i.e., Slope_{F_V/F_M} and Slope_{μ}) derived from these linear regressions were used to indicate the sensitivity of phytoplankton to an increase in temperature (Mai et al. 2021). Moreover, we estimated the effect of annual integrated effect (IE) of rising temperatures on phytoplankton assemblages (Li. et al 2015; Chen et al. 2023) as:

$$IE(\%) = \frac{\int_{d=0}^{d=365}[\text{Chl } a]\times(e^{\mu}-1)\times\text{Slope}_{\mu}}{\int_{d=0}^{d=365}[\text{Chl } a]\times(e^{\mu}-1)}\times 100\% \quad (6)$$

where e^{μ} presents the exponential function of growth rate and the *IE* indicates the effect of annual 1°C increase in temperature on the biomass of larger and smaller cell assemblages.

2.6. Field environmental and biological measurements

At each experimental time of the year, surface seawater temperature (SST) and salinity (SSS) were measured prior to sampling using a multiparameter water quality monitor sonde (YSI 6600, Yellow Springs Instruments, Yellow Springs, USA), and photosynthetically

active radiation (PAR) and air temperature were acquired from European Centre for Medium-Range Weather Forecasts (https://cds.climate.copernicus.eu/). According to meteorological industry standards, we defined summer with an average daily temperature equal to or higher than 22 ºC (i.e., Julian Day 175-263, 2022 and Julian Day 157-212, 2023), and the winter with temperature less than 10 ºC (i.e., Julian Day 334 to next Julian Day 92).

Concentration of ammonia (NH_4^+), nitrite (NO_2^-), nitrate (NO_3^-), phosphate (PO_4^{3-}) and silicate (SiO_3^{2-}) were measured using an automatic nutrient analyzer (AA3, Seal, Germany) (Hansen and Koroleff 2007), and the dissolved inorganic nitrogen (DIN) concentration was calculated by summing NH_4^+, NO_2^- and NO_3^-.

To determine Chl *a* concentration at sampling site, 500 mL of natural seawater was sequentially filtered onto PC filters with 20 and 0.2 μm pore sizes. The filters containing larger (>20 μm) and smaller phytoplankton cells (<20 μm) were extracted and Chl *a* content was measured as described above. The proportions of chlorophyll *a* made up by larger and smaller phytoplankton cells were calculated as

$$>20\ \mu m\ (\%) = \text{Chl } a_{(>20\ \mu m)}/[\text{Chl } a_{(>20\ \mu m)}+\text{Chl } a_{(<20\ \mu m)}] \quad (7)$$

$$<20\ \mu m\ (\%) = \text{Chl } a_{(<20\ \mu m)}/[\text{Chl } a_{(>20\ \mu m)}+\text{Chl } a_{(<20\ \mu m)}] \quad (8)$$

where Chl $a_{(<20\ \mu m)}$ and Chl $a_{(<20\ \mu m)}$ represent the Chl *a* of larger and smaller phytoplankton cells, respectively.

To measure picophytoplankton abundance, surface seawater was pre-filtered through a PC filter with a pore size of 20 μm, filled into 2-mL cryotubes and fixed with 50%

glutaraldehyde solution to a final concentration of 1% (v/v). After shaking for complete mixing, the cryotubes were kept in the dark for 20 min, then frozen and stored in liquid nitrogen until analysis. Pico-eukaryotes (Euk) and *Synechococcus* (*Syn*) were identified and quantified using an Accuri C6 flow cytometer (Becton-Dickinson, USA) with 1 μm diameter yellow-green latex beads (Polysciences Co., USA) as internal standards. The Euk and Syn were distinguished based on side scattering (SSC) compared to FL3 (red fluorescence) and FL2 (orange fluorescence) compared to FL3 signals (Jiang et al. 2017; Wei et al. 2019). Samples were run at a slow flow rate on the Accuri C6 and the raw data were acquired, saved and analyzed using FlowJo software.

To determine phytoplankton composition, 500 mL of natural seawater was sequentially filtered onto PC filters with 20 and 0.2 μm pore sizes. The cell collections retained by filters were transferred to 2-mL cryotubes, flash-frozen in liquid nitrogen and stored at -80 ºC until analysis. DNA was extracted using the FastDNA SPIN kit (MP Biomedicals, California, USA) and amplicon sequencing was performed using the V4 region of 18S rDNA amplified with primers 528F (5'-GCGGTAATTCCAGCTCCAA-3') and 706R (5'-AATCCRAGAATTTCACCTCT-3') on Illumina Hiseq 2500 platform at Tianjin Novogene Bioinformatic Technology Co., Ltd. (Tianjin, China). Sequence denoization and assembly were performed using QIIME 2 (Bolyen et al. 2019), and the operational taxonomic unit (OTU) tables were then generated with quality control by DADA2 (Robeson et al. 2020). Representative sequences were annotated according to Silva 138 database to obtain OTU

classification information for phytoplankton composition analysis. To further analyze the eukaryotic microalgal community, non-algal OTUs, containing OTUs of Chytridiomycota, Arthropoda, Mollusca, Ciliophora, etc. were removed.

2.7. Statistical analysis

Data are presented as mean and standard deviations (mean ± SD). To determine whether the diversity of the community correlates with its temperature sensitivity, the Simpson index, which indicates the probability that two random individuals belong to different species, was calculated according to Simpson (1949):

$$\text{Simpson Index}=1-\frac{\sum n(n-1)}{N(N-1)} \tag{9}$$

where n represents the total number of organisms of a particular species and N represents the total number of organisms of all species

Paired t-test (Prism8, GraphPad software) was used to detect significant differences between the parameters (F_V/F_M, μ, $Slope_{F_V/F_M}$, $Slope_{\mu}$, α, and E_K) of larger and smaller phytoplankton cells. The model of Thomas et al. (2012) was used to fit the thermal performance curves (TPCs) using packages "rTPC" version 1.0.5, "nls.multstart" version 1.3.0 (Padfield et al. 2020) and "tidyverse" version 2.0.0 (Wickham et al. 2019) in R software:

$$\mu=a\times e^{b\times T}\times\left(1-\left(\frac{T-z}{c}\right)^2\right) \tag{10}$$

where a, b, and z are shape parameters, c indicates thermal niche width and T indicates temperature.

To identify the main factors regulating temperature sensitivity, all environmental variables were analyzed with redundancy analysis (RDA) using "rda" function in "vegan" package (Oksanen et al. 2007). Analysis of covariance (ANCOVA) was performed using SPSS to correct for the influence of nutrients content on phytoplankton responses temperature rise.

3. Results

3.1. Annual changes of field physico-chemical environments

The daily doses of photosynthetically active radiation (PAR), temperature and nutrient concentrations in Laoshan Bay during the study period - Julian day 177, 2022 to Julian day 211, 2023 (June 26, 2022 to July 30, 2023) - are shown in Fig. 2. The PAR level varied between 0.76 and 11.6 MJ m^{-2} (Fig. 2A) and the air temperature varied between -8.34 and 30.1 ºC (Fig. 2B). Fluctuation of the values indicated a frequent cloudy or rainy day at sampling site, especially in summer. Surface seawater temperature (SST) showed a similar range and seasonal variation to air temperature, while salinity (SSS), which ranged from 30.2 to 32.3, showed an opposite seasonal variation to SST (Fig. 2B). The concentrations of dissolved inorganic nitrogen (DIN) varied between 0.09 and 11.9 μmol L^{-1}, with the highest DIN and NO_3^- values occurring in autumn (Fig. 2C), and that of phosphate (DIP, 0

- 0.69 μmol L^{-1}) and silicate (DSi, 0 - 9.56 μmol L^{-1}) followed a similar seasonal variation as the DIN (Fig. 2D).

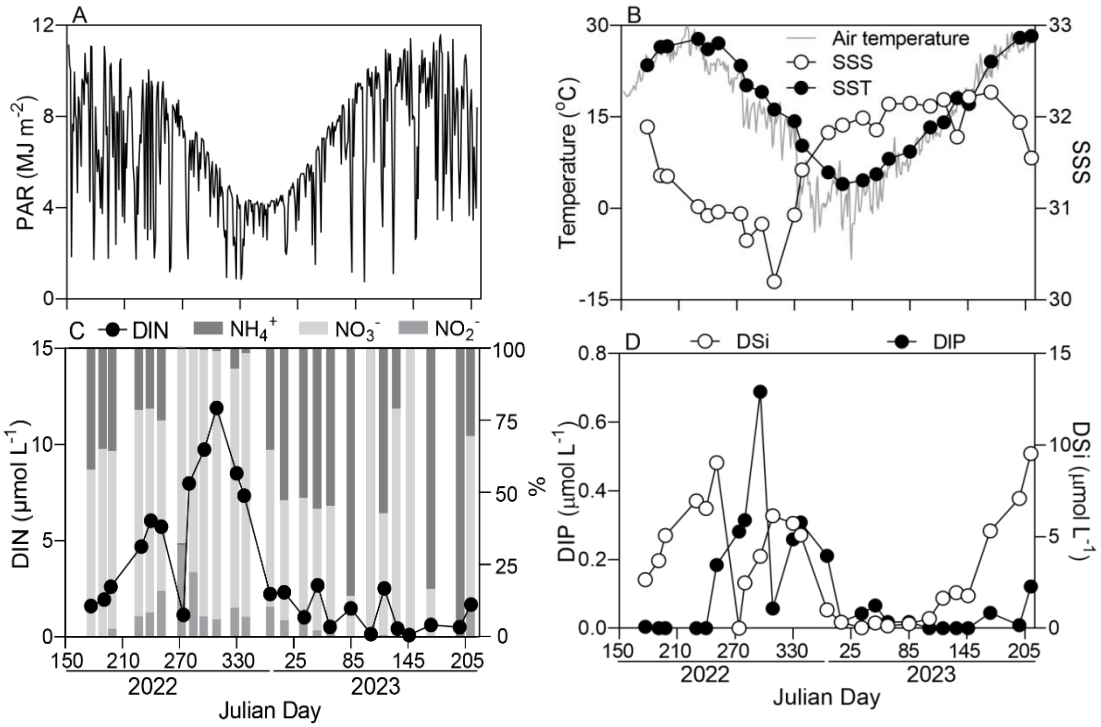

Fig. 2. Daily variation of physico-chemical factors in Laoshan Bay during Julian day 160, 2022 to Julian day 206, 2023: A) photosynthetically active radiation dose (PAR, MJ m^{-2}), B) temperature (°C) in air and surface seawater (SST), and surface seawater salinity (SSS), C) nutrient concentrations of dissolved inorganic nitrogen (DIN) and the proportion of ammonium (NH_4^+), nitrate (NO_3^-) and nitrite (NO_2^-), and D) dissolved inorganic phosphate (DIP) and silicate (DSi).

3.2. Annual changes of phytoplankton community

During the study period, the *in situ* phytoplankton biomass (Chl *a*) varied between 0.84 ± 0.04 and 7.76 ± 0.65 μg L^{-1}, with the proportion of smaller phytoplankton cells varying

between 18% and 96% (Fig. 3A). The highest Chl *a* concentration presented in winter (Julian day 365), with a lower proportion (25%) of smaller cells. Smaller phytoplankton cells generally dominated in this area, with *Synechococcus* (*Syn*) varying between 3.49×10^{6} and 6.92×10^{8} cell mL^{-1} in winter and summer, respectively, and eukaryotes (Euk) varying between 2.26×10^{6} and 1.39×10^{8} cell mL^{-1} (Fig. 3B). In addition, the diversity of eukaryotic larger cell assemblages (Simpson index) varied between 0.08 and 0.98 throughout the year, with a higher proportion of diatoms in winter and dinoflagellates in summer (Fig. 3C). Simpson index of eukaryotic smaller cell assemblages varied between 0.78 and 0.96, with dinoflagellates and diatoms accounting for 21%-87% (Fig. 3D). More information at genus level was shown in supplemental Fig. S1.

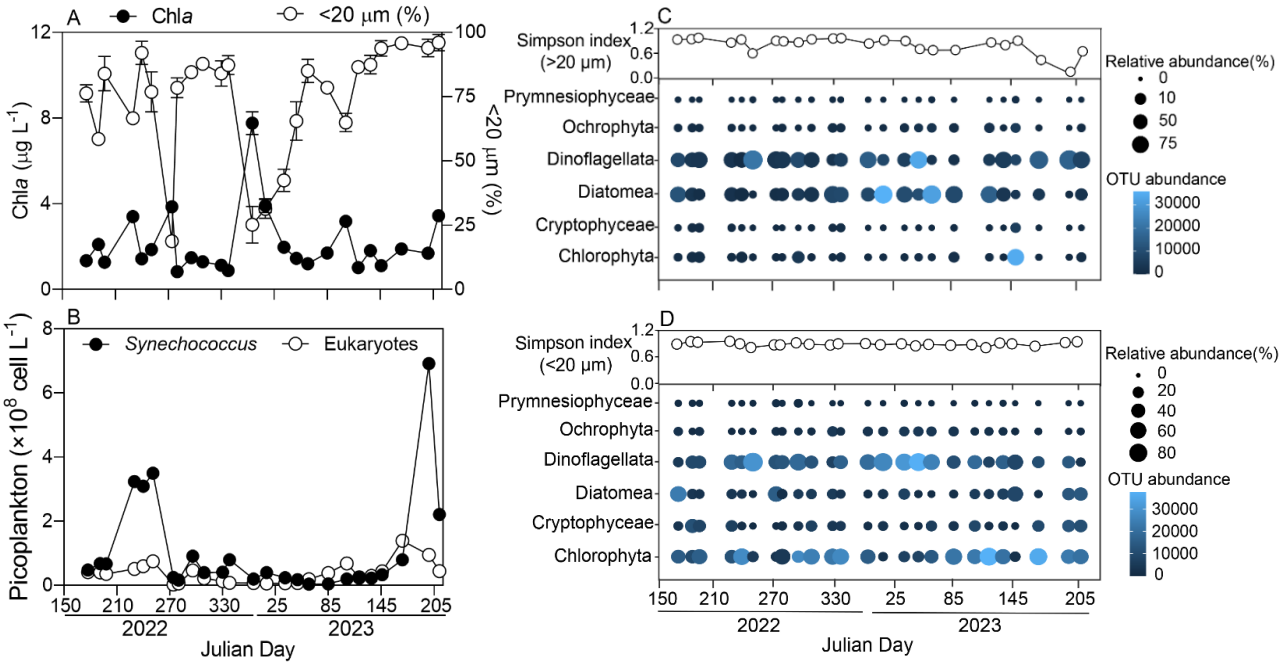

Fig. 3. Annual variation of total chlorophyll a biomass (A, Chl *a*, μg L^{-1}) in surface seawater of the sampling site and the allocation (%) of smaller cell-size-fractionated Chl *a* (<20 μm), cell abundance of *Synechococcocus* and eukaryotes (B, cell L^{-1}) and eukaryotic community structures of larger (C, >20 μm) and smaller phytoplankton assemblages (D, <20 μm) at phylum level. Vertical bars in panel A show the standard deviations (n = 3) that often fall within the symbols.

3.3. Annual changes of phytoplankton physiology

The maximum photochemical quantum yield (F_V/F_M) of PSII of larger field phytoplankton assemblages, measured at ambient temperature in laboratory, varied between 0.15±0.02 and 0.52±0.01 during the experimental period (Fig. 4A). The F_V/F_M of smaller phytoplankton assemblages was 18% lower than their larger counterparts (Paired t-test, t = 3.11, p = 0.0049) (Fig. 4B) and was significantly higher in summer than in winter (p = 0.0016) (Fig. 4A). Accordingly, the light utilization efficiency (α) and saturation light (E_K) derived from the rapid light curve (RLC) showed a similar seasonal trend as the F_V/F_M (Fig. S2) and were higher in larger than smaller cells (Paired t-test, t = 3.63, p = 0.0014 for α; t = 3.55, p = 0.0017 for E_K). Moreover, the specific growth rate (μ) of larger cell assemblages at ambient temperature varied from -0.21±0.05 to 0.91±0.12 d^{-1} during the studied period and was lower in winter than in summer (Fig. 4C). The μ of smaller cell assemblages were about 60% lower than that of larger cell assemblages (Paired t-test, t = 5.078, p < 0.0001) (Fig. 4D) and they both showed a similar seasonal variation (Fig. 4C).

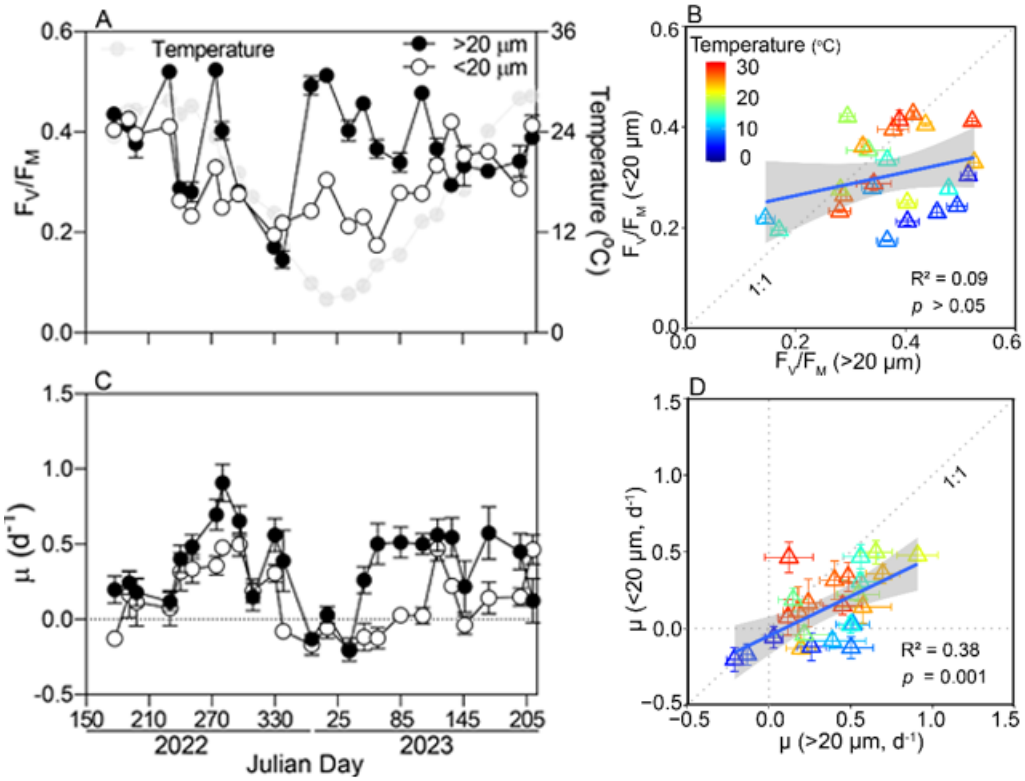

Fig. 4. Annual variation of the maximum photochemical quantum yield (A, F_V/F_M) of Photosystem II (PS II) and the specific growth rate (C, μ, d^{-1}) of larger (>20 μm) and smaller phytoplankton assemblages (<20 μm) at sampling site, and comparison of F_V/F_M (B) and μ (D) in larger cells and smaller cells from June 26, 2022 (Julian Day 177) to July 30, 2023 (next Julian Day 211). The data were obtained in laboratory at ambient temperature. The blue line in panels B and D shows the linear regression between larger cell and smaller cell assemblages with the shadow indicating 95% confidence level, and the color scale of the symbol indicates ambient temperature. Data are expressed as mean ± SD (n = 3).

3.4. Annual changes of temperature sensitivity of phytoplankton

The sensitivity to temperature rise was approximated using the "Slope" resulting from the linear fits of F_V/F_M or μ to temperature (Fig. S3 and S4, Table S1 and S2), presenting an apparent seasonal and size variations (Fig. 5). Both the $Slope_{F_V/F_M}$ and $Slope_{\mu}$ of larger and smaller cell assemblages showed a clear seasonal trend, i.e. higher in winter and lower in summer (Fig. 5AC). Moreover, the negative values of $Slope_{F_V/F_M}$ of both cell assemblages occurred in summer but positive in winter (Fig. 5A), indicating an inhibited effect of temperature rise on photosynthetic capacity in former season but a stimulating effect in later season. A comparison of the $Slope_{F_V/F_M}$ of larger cells with smaller cells showed that the stimulatory effect was greater in larger cells and the inhibitory effect was weaker in smaller cells (Fig. 5B). The $Slope_{\mu}$ showed a same seasonal trend as the $Slope_{F_V/F_M}$ (Fig. 5C), as did the differential responses of smaller and larger cells to temperature rise (Fig. 5D). In addition, using the μ and $Slope_{\mu}$ we approximately estimated the integrated effect (IE) of a 1 ºC temperature increase over one year on the primary production of phytoplankton. The IE of larger and smaller cell assemblages was -5.45% and -3.68%, respectively, indicating a negative effect of temperature increase on phytoplankton in the study area. Moreover, the $Slope_{F_V/F_M}$ and $Slope_{\mu}$ of both larger and smaller cell assemblages were negatively correlated with ambient temperature, DSi concentration and PAR (Fig. 6), and the ambient temperature was identified as one of a potentially main driver to regulate phytoplankton responses to temperature rise, followed

by DSi and PAR in Laoshan Bay. There were also significant effects of ambient temperature on $Slope_{F_V/F_M}$ and $Slope_{\mu}$ through the analysis of covariance to correct for the influence of nutrient concentrations (Table S3).

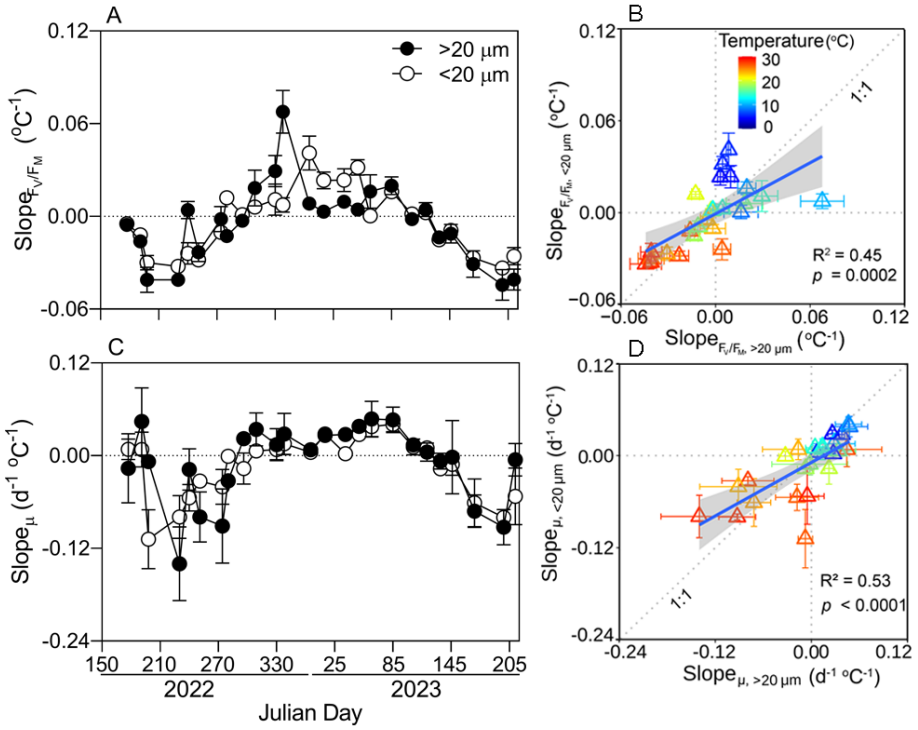

Fig. 5. Annual variation of the temperature sensitivity of photosynthetic efficiency (A, $Slope_{F_V/F_M}$, $^oC^{-1}$) and growth rate (C, $Slope_{\mu}$, d^{-1} $^oC^{-1}$) in larger (>20 μm) and smaller phytoplankton assemblages (<20 μm), and the comparison of temperature sensitivity in larger cells and smaller cells (B, $Slope_{F_V/F_M}$; D, $Slope_{\mu}$). Each slopes is derived from each temperature manipulation experiment. The blue line in panels B and D shows the linear regression of temperature sensitivity between larger and smaller cell assemblages with the shadow indicating 95% confidence level, and the color of the symbol indicates ambient temperature. Data are expressed as mean ± SD (n = 3).

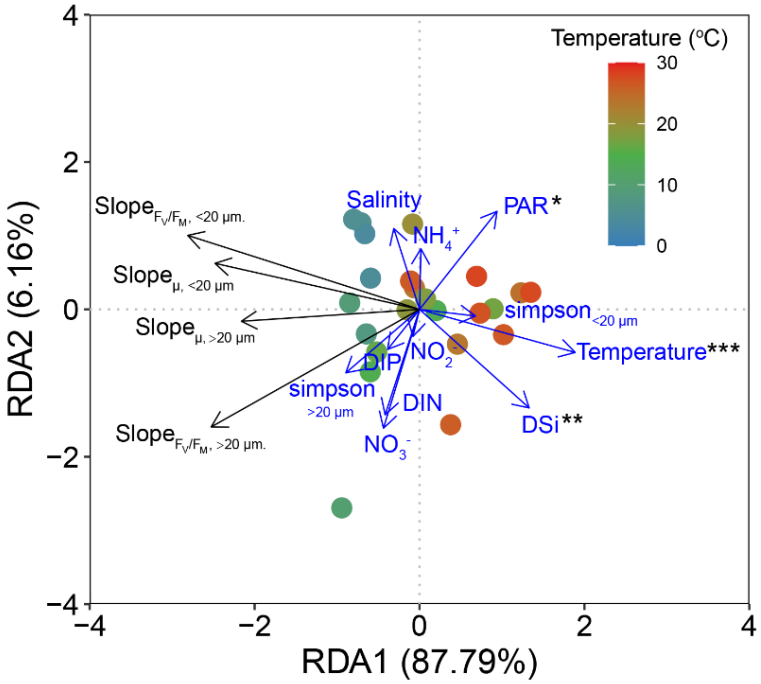

Fig. 6. Redundancy analysis (RDA) to correlate temperature sensitivity with environmental factors for larger (>20 µm) and smaller phytoplankton assemblages (<20 µm). The constrained axes RDA1 and RDA2 account for 87.79% and 6.16% of the total variance, respectively. The color in the symbols indicates the field temperature.

3.5. Thermal traits of larger and smaller phytoplankton

The thermal performance curves (TPCs) of phytoplankton assemblages by plotting the µ of pooled species assemblages against temperature showed that larger and smaller cells responded to temperature changes through different thermal traits (Fig. 7, Table 1). The optimum growth temperature (T_{opt}) of larger cell assemblages was 17.8±0.82 °C, about 20% lower than that of smaller cell assemblages, while the niche width (c) of larger cells was

27.1±1.60 ºC, about 30% wider than that of smaller cells. Accordingly, the minimum critical temperature (CT_{min}, 5.57±0.06 ºC) of larger cells was about half that of smaller cells (10.0±0.08 ºC), while the maximum critical temperature (CT_{max}) showed no significant difference between them ($p > 0.05$).

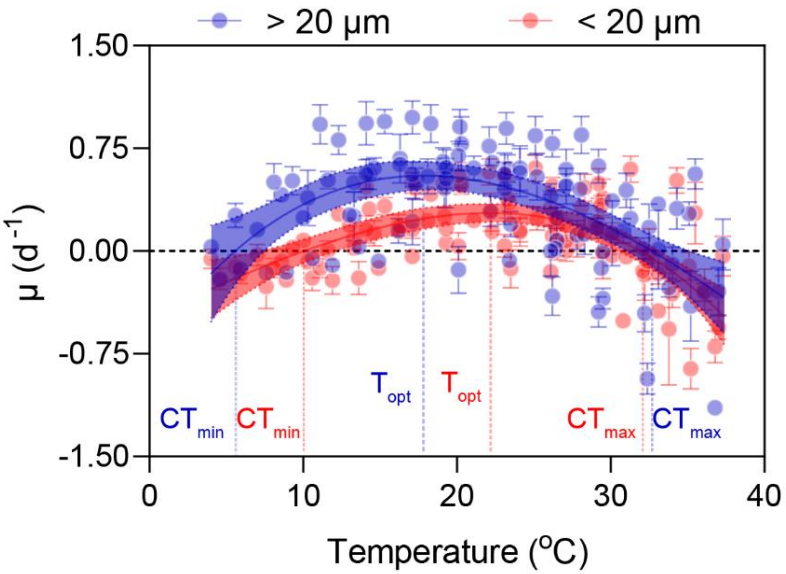

Fig. 7. The pooled growth rate (µ, d^{-1}) as a function of temperature, i.e., the thermal performance curves (TPCs) of larger (>20 µm) and smaller phytoplankton assemblages (<20 µm). The blue and red lines show the lines fitted to the TPC for larger and smaller cell assemblages, respectively. Data are expressed as mean ± SD (n = 3), and there is a total of 400 data points.

Table 1. Comparisons of parameters derived from the thermal performance curves between larger (>20 µm) and smaller phytoplankton assemblages (<20 µm), i.e., optimal growth

temperature (T_{opt}, ^{o}C), niche width (c, ^{o}C), and minimum (CT_{min}, ^{o}C) and maximum critical temperatures (CT_{max}, ^{o}C). Different letters in superscript indicate the significant difference between larger and smaller cell assemblages ($p < 0.05$).

Parameters	Larger phytoplankton (>20 μm)	Smaller phytoplankton (<20 μm)
T_{opt}	17.8 ± 0.82^{a}	22.1 ± 0.72^{b}
c	27.1 ± 1.60^{a}	21.9 ± 1.16^{b}
CT_{min}	5.57 ± 0.06^{a}	10.0 ± 0.08^{b}
CT_{max}	32.7 ± 1.54^{a}	31.9 ± 1.24^{a}

4. Discussion

We found that the effects of temperature rise on phytoplankton assemblages in Laoshan Bay varied greatly throughout the year and depended mainly on field temperature, DSi concentration and PAR level, which is consistent with previous reports (i.e., Liu et al. 2019). We also found that an increase in temperature stimulated the growth of larger phytoplankton cells (>20 μm) more strongly than their smaller counterparts (<20 μm) in winter, but inhibited it more in summer. These indicated a higher temperature sensitivity of larger than smaller phytoplankton cells and the competitive advantages of larger cells in winter but smaller cells in summer. This is in contrast to the results of Chen (2015) and Chen and Laws (2017) who used a single phytoplankton phylum.

4.1. Seasonal variations of phytoplankton community and physiology

Phytoplankton biomass and composition in temperate oceans are often subject to strong seasonal variations due to the contrasting changes in environmental factors in different seasons. As expected, the phytoplankton community in Laoshan Bay exhibited distinct temporal dynamics, which could be supported by the significant succession of larger cells from dinoflagellates to diatoms from summer to winter (Fig. 3C) and smaller cells from chlorophytes and diatoms to dinoflagellates (Fig. 3D). Such temporal dynamics in phytoplankton community structure have also been observed in other regions, such as Jiaozhou Bay (Liu et al. 2022) and the North Sea (Kase et al. 2020). The sequencing of 18S cannot detect the change in prokaryotic diversity. Considering photosynthetic prokaryotes, such as *Syn* that usually dominate in all ocean habitats (Komárek et al. 2020), we found *Syn* erupted in Laoshan Bay in summer months when nutrients are low (Fig. 3B). This corresponds to the ecological phenomenon that larger diatoms, such as *Thalassiosira* and *Bacillariophyceaes* species, often contribute to triggering blooms in temperate waters during winter and early spring when nutrients are higher and mixing depth is deeper (Horner et al., 2005; Jung et al., 2009). In contrast, smaller diatoms, such as *Cyclotella* species, prone to dominate in warmer, stratified waters during late spring and summer, as their higher surface-area-to-volume ratio provides a competitive advantage under nutrient-limited conditions (Kong et al., 2021; Liu et al., 2024).

Here, too, a seasonal change in phytoplankton biomass was observed, which was higher

in winter than in the other seasons (Fig. 3A). According to Wang et al. (2021), the DIP/DIN ratio in the Yellow Sea (i.e., ~0.033) was much lower than the Redfield ratio of 0.063. In the present study, DIN and DIP contents were both low in winter, which may cause the low growth rate of phytoplankton in winter in Laoshan Bay (Fig. 4C). Of course, the low temperature in winter could also be responsible for the low growth rate due to the low activities of cellular enzymes (Rehder et al. 2023), which is consistent with the coupling of temperature and growth rate found here on a seasonal scale ($R^2 = 0.59$, $p<0.05$) (Figs. 2B and 4C) and in other studies (Feng et al. 2021). However, the low growth rate of larger and smaller phytoplankton in winter was unexpectedly not coupled with the high biomass (Fig. 3A), which could be explained by the stronger limitation of zooplankton predation by low temperatures (Liu et al. 2023, Rose and Caron 2007).

The high growth rate of phytoplankton in spring and autumn (Fig. 4C) is supported by their high metabolic efficiency at suitable temperatures (Thomas et al. 2012); however, the lower growth rate in summer is not coupled with higher F_V/F_M (Figs. 4AC). Previous studies have shown that the activation energy of photosynthesis is lower than that of respiration (Barton et al. 2018). Therefore, the increase in temperature may reduce the allocation of photosynthate for growth due to increased respiratory consumption (Barton er al. 2020). In the present study, the high photosynthetic capacity was possibly compensated by a higher respiratory consumption, resulting in a lower growth rate. The low growth rate in winter was in an uncoupled relationship with their high F_V/F_M (Fig. 4A).

This may have been exacerbated by the decreasing DIP, DIN and DSi levels, which could not sufficiently support the synthesis of biological macromolecules and hinder cell division and phytoplankton growth. This discrepancy was also observed in previous reports (Li and Campbell 2016, Gorbunov and Falkowski 2021).

4.2. Seasonal dynamics of the effect of rising temperatures on phytoplankton assemblages

It is known that rising temperatures influence cell physiological and biochemical processes of phytoplankton, e.g. by altering enzymatic activity and mitochondrial respiration, and thus growth (Schaum et al. 2017; Rehder et al. 2023). Our results supported this and also indicated a positive effect of temperature increase on the growth of winter phytoplankton assemblages in the field and a negative effect on summer phytoplankton assemblages (Fig. 5). In winter with low temperatures, the activity of cellular enzymes, such as RubisCO, is low; this means that the cells cannot take up and assimilate enough carbon to support metabolism (Rehder et al. 2023), which in particular worsens respiration and thus leads to an overall decline in cell growth (Barton 2018). In this situation, it is understandable that a moderate increase in temperature favors the growth of phytoplankton by activating cellular enzymes and thus increasing photosynthesis, as found here (Fig. 5) or in other studies (Jabre et al. 2020). In summer however, there was a temperature rise-related decline in photosynthetic activity and the growth rate of the cell assemblages in Laoshan Bay (Fig. 5). This could be due to the fact that the increased stimulation of respiration by a further increase in temperature is not conducive to the accumulation of carbon in cells, possibly

leading to a reduction in growth rate (Xu et al. 2020). On the other hand, the increased temperature in summer could also increase the production of cellular reactive oxygen species, which are generally believed to attack the photosynthetic structural proteins and enzymes, such as D1 protein and RubisCO, damaging the photosynthetic apparatus of phytoplankton and thus reducing its photosynthetic activity (Barton 2018; Deschaseaux et al. 2019).

4.3. Differential temperature sensitivities of larger and smaller phytoplankton assemblages

Larger and smaller phytoplankton cells are known to respond differently to an increase in temperature (Xu et al. 2020; Fan et al. 2023). This was also indicated by the thermal traits derived from the thermal performance curves obtained by plotting the pooled μ against temperature (Fig. 7). Larger cells have a lower optimal growth temperature (T_{opt}) and wider niche width (c) than their smaller counterparts, as well as a lower minimum critical temperature (CT_{min}, Table 1). In winter with low ambient temperature, larger cells might have a greater competitive advantage than smaller ones, as shown by their lower CT_{min} (Table 1) and higher temperature sensitivity (Fig. 5). This could be due to the fact that larger cells have more space to store more active substances such as enzymes (Finkel et al. 2010) and thus maintain certain physiological activities at low temperatures, which could explain their lower CT_{min} (Fig. 7 and Table 1). Both the ambient temperature and the elevated temperature in winter were still higher than the CT_{min} of the larger cells, therefore the

elevated temperature stimulates their growth more than that of the smaller cells. The wider temperature of resistance (c) of larger cells indicated their greater resistance to fluctuations in ambient temperature, as compared to smaller cells. Although this condition occurs in the field after long-term acclimatation, which is different from the mimic acute temperature increase investigated in this study.

On the contrary, smaller cells have a higher T_{opt} and narrower c, as well as a higher CT_{min} (Table 1). In summer with high ambient temperature, they exhibited a competitive advantage in coping with rising temperature than larger ones, as evidenced by a higher T_{opt} and a weaker inhibitory effect, i.e., higher $Slope_{F_V/F_M}$ and $Slope_{\mu}$ (Figs. 5BD and 7). This could be due to smaller cells such as *Thalassiosira pseudonana* and *Chlorella vulgaris* meeting growth requirement more energy efficiently, for example by altering RubisCO activity and down-regulating respiration (Li and Campbell 2017, Padfield et al. 2015, Xu et al. 2020), suggesting that they would achieve rapid adaptation to temperature rise within the survivable range. Moreover, smaller cells have a higher surface area-to-volume ratio, higher gene density and genes potentially involved in stress resistance and nutrient uptake, which could contribute to their success in ever-changing environment (Cuvelier et al. 2010). Similarly, there is a competitive advantage of smaller cells over larger cells in summer as temperatures rise in this study. Due to the inconsistent responses of larger and smaller cells to temperature rise, the composition of phytoplankton would change with an increase in temperature. Furthermore, our results showed a decrease of 5.45% and 3.68% by a 1 ºC

increase over a year for larger and smaller cells, respectively, indicating the negative effects of the temperature increase and thus the loss of marine phytoplankton biomass. This study is based on laboratory temperature rise experiments, and we suggest that future researches should be conducted by combing rigorous mesocosm and field experiments.

Author contribution statement

W. Z.: Writing original draft, Methodology, Investigation and Data curation. J. L.: Validation, Resources, Methodology, Investigation, Data curation and Funding acquisition. T. L.: Validation, Data curation and Conceptualization. H. S.: Writing original draft, Validation, Funding acquisition and Conceptualization. B. C.: Methodology, Investigation, Data curation and Writing original draft. B. C.: Validation, Supervision. G. L.: Writing - review & editing, Writing original draft, Validation, Supervision, Funding acquisition and Conceptualization.

Declaration of competing interest

None declared.

Data Availability

All relevant data are in the paper and its Supporting Information.

Acknowledgment

We are thankful for the help of G. M. Mai and H. W. Ren for data analysis. This work was supported by the National Key R&D Program of China (2024YFF0507000), Key Research and Development Program of Shandong Province (2020ZLYS04), National Natural Science Foundation of China (32371665), and Ocean Negative Carbon Emissions (ONCE) Program.

References

Aflenzer, H., L. J. Hoffmann, T. M. Holmes, K. Wuttig, C. Genovese, and A. R. Bowie. 2023. Effect of dissolved iron (II) and temperature on growth of the Southern Ocean phytoplankton species *Fragilariopsis cylindrus* and *Phaeocystis antarctica*. Polar Biol. **46**: 1163-1173. doi:10.1007/s00300-023-03191-z

Bai, Y., D. Pan, X. He, and F. Gong. 2005. Ocean primary production estimation of China Bohai Sea and Yellow Sea by HY-COCTS. SPIE **5977**: 25-33. doi:10.1117/12.627455

Barton, S. 2018. Understanding the responses of marine phytoplankton to experimental warming. (Doctor of Philosophy in Biological Sciences) the University of Exeter.

Barton, S., J. Jenkins, A. Buckling, C.E. Schaum, N. Smirnoff, J.A. Raven, and G. Yvon-Durocher. 2020. Evolutionary temperature compensation of carbon fixation in marine phytoplankton. Ecol. Lett. **23**: 722-733. doi: 10.1111/ele.13469

Bolyen, E., and others. 2019. Reproducible, interactive, scalable and extensible microbiome data science using QIIME 2. Nat. Biotechnol. **37**: 852-857. doi:10.1038/s41587-019-0209-9

Chen, B. and E.A. Laws. 2017. Is there a difference of temperature sensitivity between marine phytoplankton and heterotrophs? Limnol. Oceanogr. **62**: 806-817. doi:10.1002/lno.10462

Chen, B. 2015. Patterns of thermal limits of phytoplankton. J. Plankton Res. **37**: 285-292. doi:10.1093/plankt/fbv009

Chen, B., Song, H., Yang, X., Xu, G., Zhao, W., Meng, Y., Li, G. 2023. Decreasing O_2 availability reduces cellular protein contents in a marine diatom. Sci. Total Environ. **887**:164032. doi:10.1016/j.scitotenv.2023.164032

Chen T, Zhang Y, Song S., and N. Chen. 2022. Diversity and seasonal variation of marine phytoplankton in Jiaozhou Bay, China revealed by morphological observation and metabarcoding[J]. J. Oceanol. Limn. **40**: 577-591. doi:10.1007/s00343-021-0457-7

Cheng, L., and others. 2022. Metabolic adaptation of a globally important diatom following 700 generations of selection under a warmer temperature. Environ. Sci. Technol. **56**: 5247-5255. doi:10.1021/acs.est.1c08584

Clark, J., T. M. Lenton, H. T. P. Williams, and S. J. Daines. 2013. Environmental selection and resource allocation determine spatial patterns in picophytoplankton cell size. Limnol. Oceanogr. **58**: 1008-1022. doi:10.4319/lo.2013.58.3.1008

Cullen, J. J., and R. F. Davis. 2003. The blank can make a big difference in oceanographic measurements. Limnol. and Oceanogr. Bulletin **12**: 29-35. doi:10.1002/lob.200312229

Cuvelier M.L., and others. 2010. Targeted metagenomics and ecology of globally important uncultured eukaryotic phytoplankton[J]. Proc. Natl. Acad. Sci. U.S.A. **107**: 14679-14684. doi:10.1073/pnas.1001665107

Dalpadado, P., and others. 2023. Rapid climate change alters the environment and biological production of the Indian Ocean. Sci. Total Environ. **906**: 167342. doi:10.1016/j.scitotenv.2023.167342

Daufresne M., K. Lengfellner, U. Sommer. 2009. Global warming benefits the small in aquatic ecosystems. Proc. Natl. Acad. Sci. U.S.A. **106**: 12788-12793. doi:10.1073/pnas.0902080106

Deschaseaux, E., J. O'brien, N. Siboni, K. Petrou, and J. R. Seymour. 2019. Shifts in dimethylated sulfur concentrations and microbiome composition in the red-tide

causing dinoflagellate *Alexandrium minutum* during a simulated marine heatwave. Biogeosciences **16**: 4377-4391. doi:10.5194/bg-16-4377-2019

Dong, J.-Y., X. Wang, X. Zhang, G. Bidegain, and L. Zhao. 2023. Integrating multiple indices based on heavy metals and macrobenthos to evaluate the benthic ecological quality status of Laoshan Bay, Shandong Peninsula, China. Ecol. Indic. **153**: 110367. doi:10.1016/j.ecolind.2023.110367

Dalpadado, P., (2024). Rapid climate change alters the environment and biological production of the Indian Ocean. *Science of the Total Environment*, *906*, 167342.

Fan, J., F. Li, S. Hu, K. Gao, and J. Xu. 2023. Larger diatoms are more sensitive to temperature changes and prone to succumb to warming stress. Limnol. Oceanogra. **68**: 2512-2528. doi: 10.1002/lno.12438

Feng, J., Stige, L. C., Hessen, D. O., Zuo, Z., Zhu, L., & Stenseth, N. C. 2021. A threshold sea - surface temperature at 14 °C for phytoplankton nonlinear responses to ocean warming. Global Biogeochem. Cy. **35**: 1-13. doi: 10.1029/2020GB006808

Finkel, Z. V., J. Beardall, K. J. Flynn, A. Quigg, T. A. V. Rees, and J. A. Raven. 2010. Phytoplankton in a changing world: cell size and elemental stoichiometry. J. Plankton Res. **32**: 119-137. doi:10.1093/plankt/fbp098

Flanjak, L., and others. 2022. The effects of high temperatures and nitrogen availability on the growth and composition of the marine diatom *Chaetoceros pseudocurvisetus*. J. Exp. Bot. **73**: 4250-4265. doi:10.1093/jxb/erac145

Frölicher, T. L., and C. Laufkötter. 2018. Emerging risks from marine heat waves. Nat. Commun. **9**: 650. doi:10.1038/s41467-018-03163-6

Genty, B., J. M. Briantais, and N. R. Baker. 1989. The relationship between the quantum yield of photosynthetic electron transport and quenching of chlorophyll fluorescence. Biochim. Biophys. Acta **990**: 87-92. doi:10.1016/S0304-4165(89)80016-9

Gorbunov M.Y., and P.G. Falkowski. 2021. Using chlorophyll fluorescence kinetics to determine photosynthesis in aquatic ecosystems. Limnol. Oceanogr. **66**: 1-13. DOI:10.1002/lno.11581.

Hansen, H. P., and F. Koroleff. 2007. Determination of nutrients.

Horner, R.A., J.R. Postel, C. Halsband-Lenk, J.J. Pierson, G. Pohnert, and T. Wichard. 2005. Winter-spring phytoplankton blooms in Dabob Bay, Washington[J]. Prog. in Oceanogr. **67**:286-313. doi: 10.1016/j.pocean.2005.09.005

IPCC, 2013: Climate change 2013: the physical science basis: Working Group I contribution to the Fifth assessment report of the Intergovernmental Panel on Climate Change, *Cambridge university press*, 1535pp.

Jabre, L., A. E. Allen, J. S. P. McCain, and E. M. Bertrand. 2020. Molecular underpinnings and biogeochemical consequences of enhanced diatom growth in a warming Southern Ocean. Proc. Natl. Acad. Sci. U.S.A. **118**: e2107238118. doi:10.1073/pnas.2107238118

Jiang, X., J. Li, Z. Ke, C. Xiang, Y. Tan, and L. Huang. 2017. Characteristics of picoplankton abundances during a Thalassiosira diporocyclus bloom in the Taiwan Bank in late winter. Mar. pollut. Bull. **117**: 66-74. doi: 10.1016/j.marpolbul.2017.01.042

Jung, S.W., O.Y. Kwon, J.H. Lee, and M.S. Han. 2009. Effects of Water Temperature and Silicate on the Winter Blooming Diatom *Stephanodiscus*

hantzschii (Bacillariophyceae) Growing in Eutrophic Conditions in the Lower Han River, South Korea. J. Freshw. Ecol. **24**:219–226. doi:10.1080/02705060.2009.9664286

Kase, L., A.C. Kraberg, K. Metfies, S. Neuhaus, P.A.A. Sprong, B.M. Fuchs, M Boersma, and K.H.Wiltsh. 2020. Rapid succession drives spring community dynamics of small protists at Helgoland Roads, North Sea. J. Plankton Res. **42**: 305 – 319. doi:10.1093/plankt/fbaa017

Kolber, Z. S., O. Prášil, and P. G. Falkowski. 1998. Measurements of variable chlorophyll fluorescence using fast repetition rate techniques: defining methodology and experimental protocols. Biochim. Biophys. Acta **1367**: 88-106. doi:10.1016/S0005-2728(98)00135-2

Komarek, J., J.R. Johansen, J. Smarda, and O. Strunecký. 2020. Phylogeny and taxonomy of Synechococcus–like cyanobacteria. *Fottea. Olomouc.* **20**:171-191. doi:10.5507/fot.2020.006

Kong X, M. Seewald, T. Dadi, F. Kurt, M. Chenxi, B. Bertram, and others. 2021. Unravelling winter diatom blooms in temperate lakes using high frequency data and ecological modeling. Water Res. **190**:116681. doi:10.1016/j.watres.2020.116681

Li G., and D. Campbell. 2017. Interactive effects of nitrogen and light on growth rates and RUBISCO content of small and large centric diatoms. Photosynthe. Res. **131**: 93-103. doi:10.1007/s11120-016-0301-7.

Liu J., X. Ding, X. Xia, L. Zhou, W. Liu, Y. Lai, and others. 2024. Dissolved organic phosphorus promotes Cyclotella growth and adaptability in eutrophic tropical estuaries[J]. Appl. Environ. Microbiol. **90**:e01637-23. doi: 10.1128/aem.01637-23

Liu, H., C. Yang, P. Zhang, W. Li, X. Yang, and X. Zhang. 2016. Demersal nekton community structure of artificial reef zones in Laoshan Bay, Qingdao. Biodiversity Sci. **24**: 896. doi:10.17520/biods.2016111

Liu K., B. Chen, S. Zhang, S. Mitsuhide, Z. Shi, and H. Liu. 2019. Marine phytoplankton in subtropical coastal waters showing lower thermal sensitivity than microzooplankton. Limnol. Oceanogr. **64**: 1103-1119. doi:10.1002/lno.11101

Liu, K., J. Nishioka, B. Chen, K. Suzuki, S. Cheung, Y. Lu, H. Wu, and H. Liu. 2022. Role of nutrients and temperature in shaping distinct summer phytoplankton and microzooplankton population dynamics in the western North Pacific and Bering Sea. Limnol. Oceanogr. 68: 649-665. doi: 10.1002/lno.12300

Liu, L., M. Fan, and Y. Kang. 2023. Effect of nutrient supply on cell size evolution of marine phytoplankton. Math. Biosci. Eng. **20**: 4714-4740

Liu S., Z. Cui, Y. Zhao, et al. 2022. Composition and spatial-temporal dynamics of phytoplankton community shaped by environmental selection and interactions in the Jiaozhou Bay[J]. Water res. **218**: 118488. doi:10.1016/j.watres.2022.118488.

Mai, G., J. Liu, X. Xia, X. Pang, and G. Li. 2021. Acutely rising temperature reduces photosynthetic capacity of phytoplankton assemblages in tropical oceans: a large-scale investigation. Front. Mar. Sci. **8**: 710697. doi:10.3389/fmars.2021.710697

Oksanen, J.I., and others. 2007. vegan: Community Ecology Package. R package version 1.8-5.

Padfield, D., H. O'Sullivan, and S. Pawar. 2020. rTPC and nls.multstart: a new pipeline to fit thermal performance curves in R. bioRxiv **12**: 1138-1143. doi:10.1111/2041-210X.13585

Padfield, D., G. Yvon-Durocher, A. Buckling, S. Jennings, and G. Yvon-Durocher. 2015. Rapid evolution of metabolic traits explains thermal adaptation in phytoplankton. Ecol. Lett. **19**: 133-142. doi:10.1111/ele.12545

Porra, R. J. 2004. The chequered history of the development and use of simultaneous equations for the accurate determination of chlorophylls a and b. Photosynthesis Res. **73**: 149-156. doi:10.1023/A:1020470224740

Rehder, L., B. Rost, and S. D. Rokitta. 2023. Abrupt and acclimation responses to changing temperature elicit divergent physiological effects in the diatom *Phaeodactylum tricornutum*. New Phytol. **239**: 1005-1013. doi:10.1111/nph.18982

Robeson, M. S., D. R. O'Rourke, B. D. Kaehler, M. Ziemski, M. R. Dillon, J. T. Foster, and N. A. Bokulich. 2020. RESCRIPt: Reproducible sequence taxonomy reference database management. PLoS Comp. Biol. **17**: e1009581. doi:10.1371/journal.pcbi.1009581

Rose J.M., and D.A. Caron. 2007. Does low temperature constrain the growth rates of heterotrophic protists? Evidence and implications for algal blooms in cold waters. Limnol. Oceanogr. **68**: 649-665. doi:10.4319/lo.2007.52.2.0886.

Schaum, C. E., and others. 2017. Adaptation of phytoplankton to a decade of experimental warming linked to increased photosynthesis. Nat Ecol. Evol. **1**: 0094. doi:10.1038/s41559-017-0094

Schuback, N., and others. 2021. Single-turnover variable chlorophyll fluorescence as a tool for assessing phytoplankton photosynthesis and primary productivity: opportunities, caveats and recommendations. Front. Mar. Sci. **8**. doi:10.3389/fmars.2021.690607

Schulhof, M.A., J. B. Shurin, S.A.J. Declerck, and D.B. Van de Waal. 2019. Phytoplankton growth and stoichiometric responses to warming, nutrient addition and grazing depend on lake productivity and cell size. Global Change Biol. **25**: 2751-2762. doi:10.1111/gcb.14660

Sepúlveda, J., and S. I. Cantarero. 2022. Phytoplankton response to a warming ocean. Science **376**: 1378-1379. doi:10.1126/science.abo5235

Silsbe, G. M., and J. C. Kromkamp. 2012. Modeling the irradiance dependency of the quantum efficiency of photosynthesis. Limnol. Oceanogr. Methods **10**: 645-652. doi:10.4319/lom.2012.10.645

Simpson, E. 1949. Measurement of Diversity. Nature **163**: 688. doi:10.1038/163688a0

Su, M., C. Yang, H. Kong, and L. Wang. 2022. Analysis of ecosystem change recent years based on Ecopath models in the Aoshan Bay ecosystem. Mar. Ecol. **43**: e12700. doi:10.1111/maec.12700

Sun, W., X. Tang, Y. Xu, Y. Liu, J. Ma, and H. Zhang. 2016. Characteristics of nutrients and eutrophication assessment of the Laoshan Bay, Qingdao. Trans Oceanol. Limnol. **6**: 45-52.

Thomas, M. K., C. T. Kremer, C. A. Klausmeier, and E. Litchman. 2012. A global pattern of thermal adaptation in marine phytoplankton. Sci. **338**: 1085-1088. doi:0.1126/science.1224836

Wang, F., and others. 2023. The seas around China in a warming climate. Nat. Rev. Earth Env. **4**: 535-551. doi:10.1038/s43017-023-00453-6

Wang J., A.F Bouwman., X. Liu, AHW Beusen, and Z. Yu. 2021. Harmful Algal Blooms in Chinese Coastal Waters Will Persist Due to Perturbed Nutrient Ratios. Environ. Sci. Technol. Lett. **8**: 276-284. doi:10.1021/acs.estlett.1c00012

Wei, Y., G. Zhang, J. Chen, J. Wang, C. Ding, X. Zhang, and J. Sun. 2019. Dynamic responses of picophytoplankton to physicochemical variation in the eastern Indian Ocean. Ecol. Evol. **9**: 5003-5017. doi:10.1002/ece3.5107

Wickham, H., and others. 2019. Welcome to the Tidyverse. J. Open Source Softw. **4**: 1686. doi:10.21105/joss.01686

Xu, G., J. Liu, B. Chen, and G. Li. 2020. Photoperiod mediates the differential physiological responses of smaller *Thalassiosira pseudonana* and larger *Thalassiosira punctigera* to temperature changes. J. Appl. Phycol. **32**: 2863–2874. doi:10.1007/s10811-020-02149-6

Yao, Y., J. Wang, J.-j. Yin, and X. Zou. 2020. Marine heatwaves in China's marginal seas and adjacent offshore waters: past, present, and future. J. Geophys. Res. **125**: e2019JC015801. doi:10.1029/2019JC015801

Zuccarini, P., D. Asensio, R. Ogaya, J. Sardans, and J. Peñuelas. 2020. Effects of seasonal and decadal warming on soil enzymatic activity in a P-deficient Mediterranean shrubland. Global Change Biol. **26**: 3698-3714. doi:10.1111/gcb.15077

Supporting Information

Figure S1. Annual variations in the proportion of the top 10 genera of diatoms (A, B), dinoflagellates (C, D, and other phyla (E, F) in larger (A, C, E, >20 μm) and smaller cell assemblages (B, D, F, <20 μm).

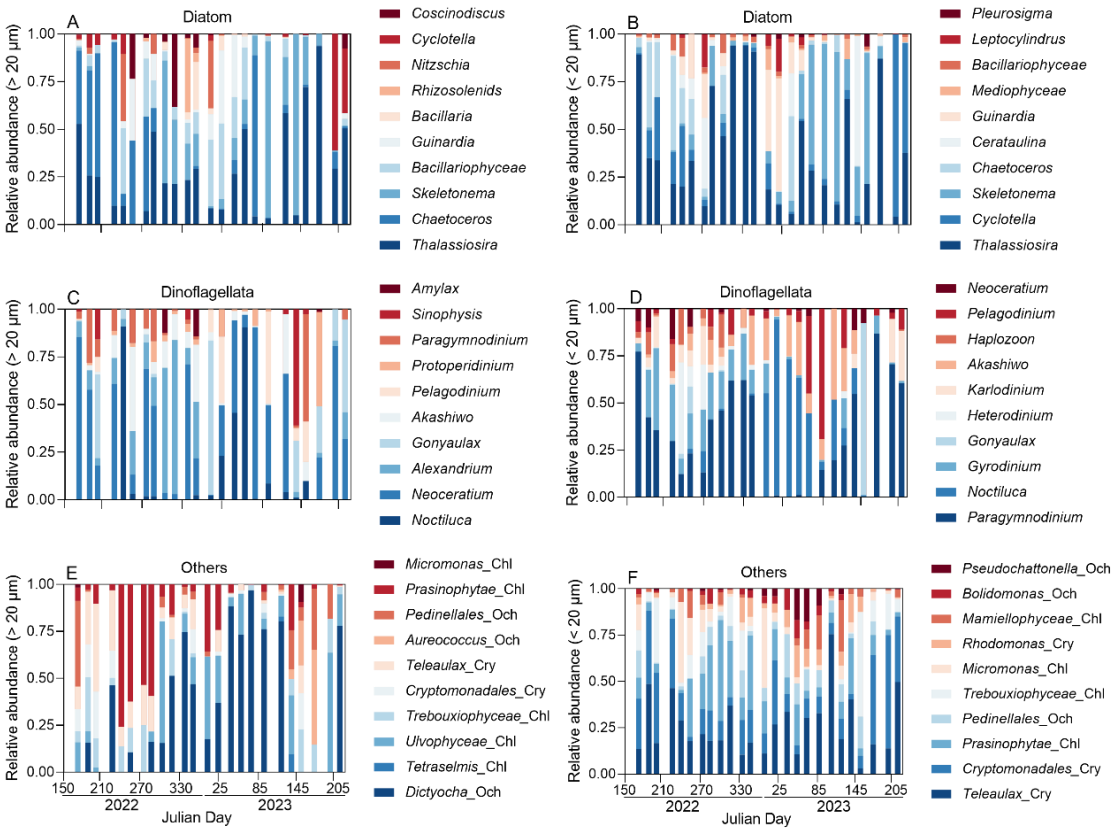

Figure S2. Photosynthetic parameters derived from the rapid light curves (RLC) of larger (>20 μm) and smaller phytoplankton assemblages (<20 μm), i.e., light utilization efficiency (A, α) and saturation irradiance (B, E_K, μmol photons m^{-2} s^{-1}) under ambient temperature. The data are expressed as mean ± SD (n = 3).

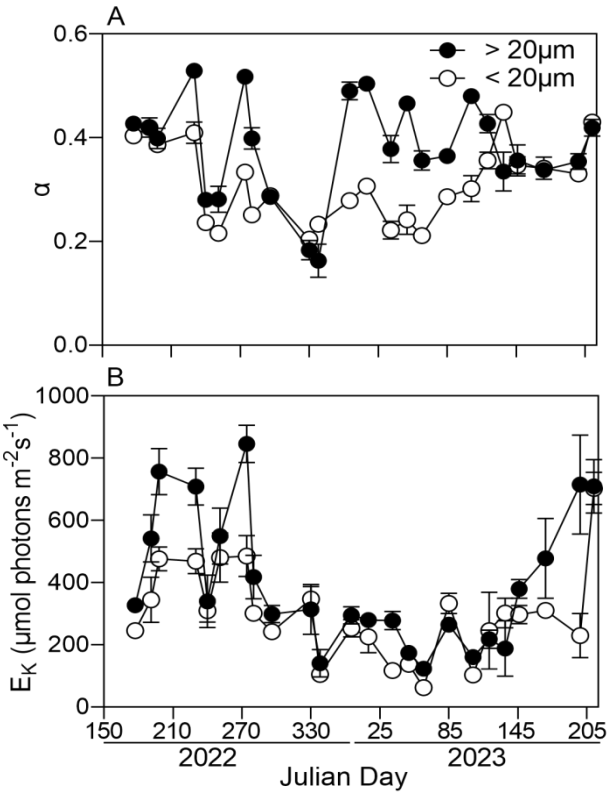

Figure S3. Photosynthetic efficiency (F_V/F_M) of larger (>20 μm) and smaller phytoplankton assemblages (<20 μm) as a function of temperature at each sampling time-point. Data are expressed as mean ± SD (n = 3). F_V/F_M are normalized to that measured at ambient temperature.

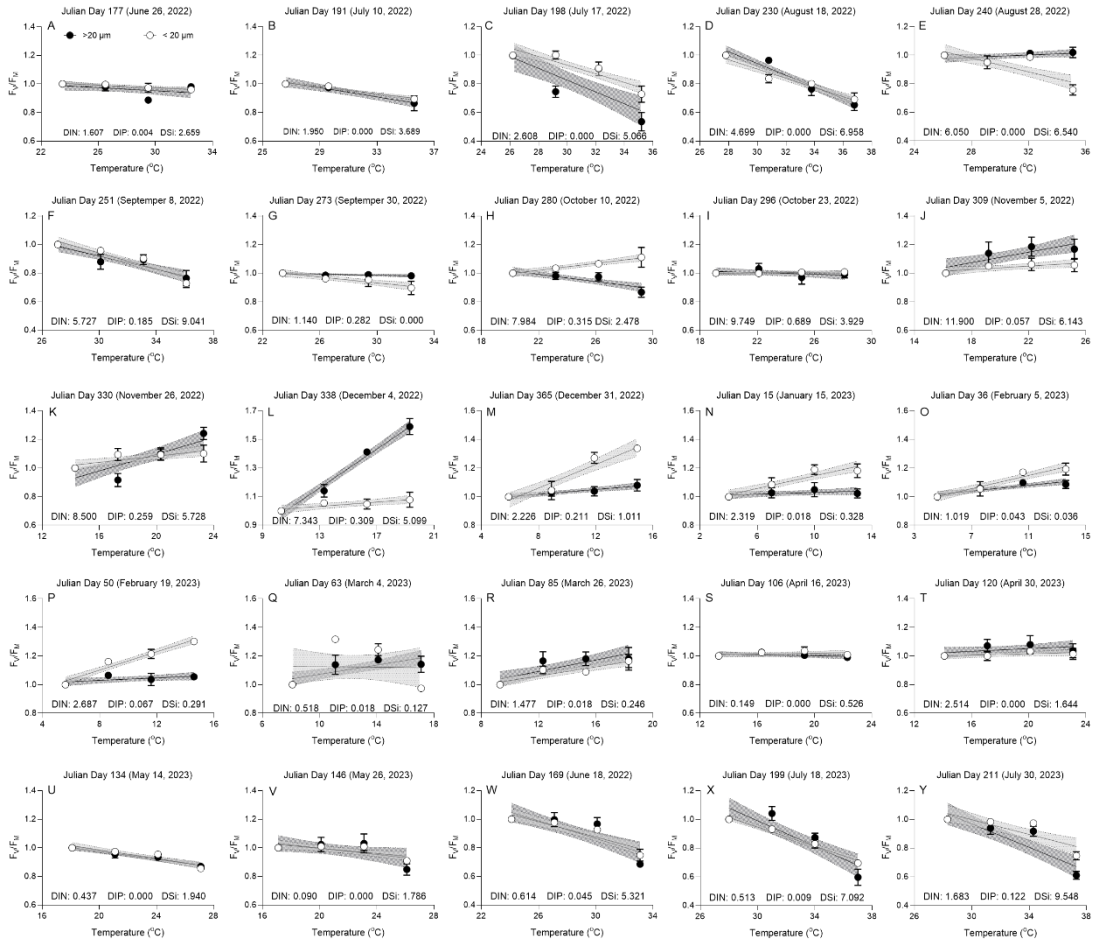

Figure. S4. Specific growth rate (μ) of larger (>20 μm) and smaller phytoplankton assemblages (<20 μm) as a function of temperature at each sampling time-point. Data are expressed as mean ± SD (n = 3).

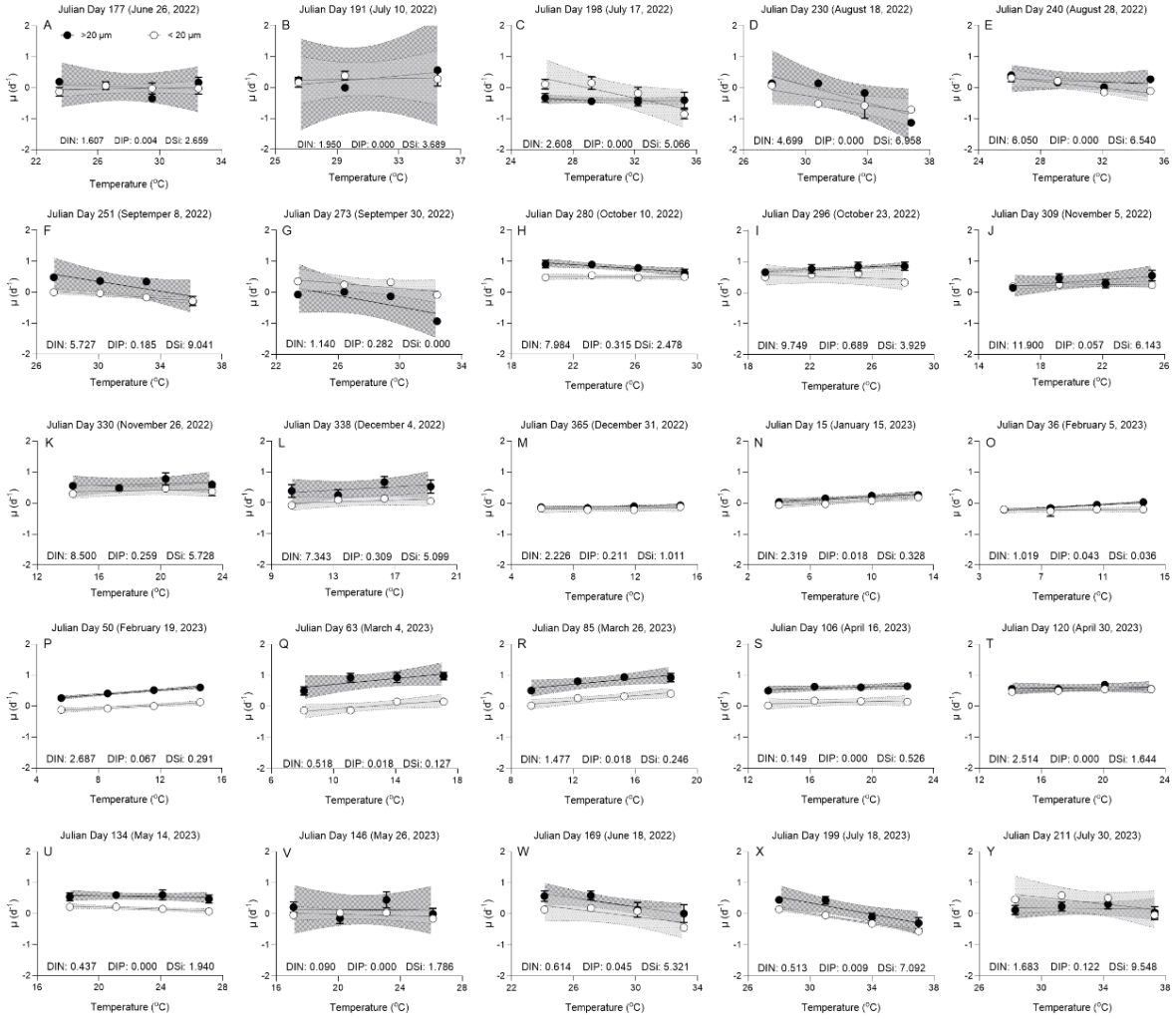

Table S1. The fitting parameters derived from the linear regressions of photosynthetic efficiency (F_V/F_M) to temperature of larger (>20 μm) and smaller phytoplankton assemblages (<20 μm).

Julian Day	Fitting parameters
177 (26-Jun, 2022)	$Slope_{(>20\ \mu m)}$ = -0.0055±0.0041, R^2 = 0.17; $Slope_{(<20\ \mu m)}$ = -0.0047±0.0023**, R^2 =0. 42
191 (10-Jul, 2022)	$Slope_{(>20\ \mu m)}$ = -0.016±0.0032***, R^2 = 0.78; $Slope_{(<20\ \mu m)}$ = -0.012±0.0014***, R^2 = 0.94
198 (17-Jul, 2022)	$Slope_{(>20\ \mu m)}$ = -0.041±0.0082***, R^2 = 0.62; $Slope_{(<20\ \mu m)}$ = -0.030±0.0047***, R^2 = 0.78
230 (18-Aug, 2022)	$Slope_{(>20\ \mu m)}$ = -0.041±0.0055***, R^2 = 0.92; $Slope_{(<20\ \mu m)}$ = -0.032±0.0039***, R^2 = 0.90
240 (28-Aug, 2022)	$Slope_{(>20\ \mu m)}$ = 0.0041±0.0055, R^2 = 0.13; $Slope_{(<20\ \mu m)}$ = -0.024±0.0069***, R^2 = 0.66
251 (8-Sep, 2022)	$Slope_{(>20\ \mu m)}$ = -0.023±0.0061***, R^2 = 0.74; $Slope_{(<20\ \mu m)}$ = -0.028±0.0031***, R^2 = 0.87
273 (30-Sep, 2022)	$Slope_{(>20\ \mu m)}$ = -0.0018±0.0081*, R^2 = 0.20; $Slope_{(<20\ \mu m)}$ = -0.010±0.0026***, R^2 = 0.55
280 (7-Oct, 2022)	$Slope_{(>20\ \mu m)}$ = -0.013±0.0025***, R^2 = 0.60; $Slope_{(<20\ \mu m)}$ = -0.012±0.0018***, R^2 = 0.70
296 (23-Oct, 2022)	$Slope_{(>20\ \mu m)}$ = -0.0029±0.0021, R^2 = 0.074; $Slope_{(<20\ \mu m)}$ = 0.00012±0.0015, R^2 = 0.12
309 (5-Nov, 2022)	$Slope_{(>20\ \mu m)}$ = 0.0018±0.012**, R^2 = 0.48; $Slope_{(<20\ \mu m)}$ = 0.0060±0.0007*, R^2 = 0.31
330 (26-Nov, 2022)	$Slope_{(>20\ \mu m)}$ = 0.029±0.010***, R^2 = 0.62; $Slope_{(<20\ \mu m)}$ = 0.011±0.010**, R^2 = 0.46
338 (4-Dec, 2022)	$Slope_{(>20\ \mu m)}$ = 0.068±0.014***, R^2 = 0.97; $Slope_{(<20\ \mu m)}$ = 0.0075±0.0048*, R^2 = 0.41
365 (31-Dec, 2022)	$Slope_{(>20\ \mu m)}$ = 0.00836±0.0014**, R^2 = 0.58; $Slope_{(<20\ \mu m)}$ = 0.041±0.011***, R^2 = 0.88
15 (15-Jan, 2023)	$Slope_{(>20\ \mu m)}$ = 0.0031±0.0018, R^2 = 0.088; $Slope_{(<20\ \mu m)}$ = 0.023±0.0054***, R^2 = 0.78
36 (5-Feb, 2023)	$Slope_{(>20\ \mu m)}$ = 0.0096±0.0025***, R^2 = 0.70; $Slope_{(<20\ \mu m)}$ = 0.0023±0.0073***, R^2 = 0.84
50 (19-Feb, 2023)	$Slope_{(>20\ \mu m)}$ = 0.0044±0.0027, R^2 = 0.21; $Slope_{(<20\ \mu m)}$ = 0.032±0.0050***, R^2 = 0.93
63 (4-Mar, 2023)	$Slope_{(>20\ \mu m)}$ = 0.016±0.011**, R^2 = 0.47; $Slope_{(<20\ \mu m)}$ = 0.0004±0.0004, R^2 = 0.00041
85 (26-Mar, 2023)	$Slope_{(>20\ \mu m)}$ = 0.020±0.0057**, R^2 = 0.54; $Slope_{(<20\ \mu m)}$ = 0.016±0.0042***, R^2 = 0.72
106 (16-Apr, 2023)	$Slope_{(>20\ \mu m)}$ = -0.0018±0.0017, R^2 = 0.086; $Slope_{(<20\ \mu m)}$ = 0.0016±0.0030, R^2 = 0.084
120 (30-Apr, 2023)	$Slope_{(>20\ \mu m)}$ = 0.0044±0.0045, R^2 = 0.11; $Slope_{(<20\ \mu m)}$ = 0.0025±0.0031, R^2 = 0.12
134 (14-May, 2023)	$Slope_{(>20\ \mu m)}$ = -0.014±0.0026***, R^2 = 0.88; $Slope_{(<20\ \mu m)}$ = -0.015±0.0021***, R^2 = 0.80
148 (26-May, 2023)	$Slope_{(>20\ \mu m)}$ = -0.0116±0.0060*, R^2 = 0.25; $Slope_{(<20\ \mu m)}$ = -0.0090±0.0036**, R^2 = 0.48
169 (18-Jun, 2023)	$Slope_{(>20\ \mu m)}$ = -0.031±0.0032***, R^2 = 0.65; $Slope_{(<20\ \mu m)}$ = -0.027±0.0043***, R^2 = 0.80
199 (18-Jul, 2023)	$Slope_{(>20\ \mu m)}$ = -0.044±0.0099***, R^2 = 0.74; $Slope_{(<20\ \mu m)}$ = -0.033±0.0030***, R^2 = 0.96
211 (30-Jul, 2023)	$Slope_{(>20\ \mu m)}$ = -0.041±0.0067***, R^2 = 0.81; $Slope_{(<20\ \mu m)}$ = -0.026±0.0057***, R^2 = 0.67

Table S2. The fitting parameters derived from the linear regression of growth rate (μ) to temperature of larger (>20 μm) and smaller phytoplankton assemblages (<20 μm).

Julian Day	Fitting parameters
177 (26-Jun, 2022)	$Slope_{(>20\ \mu m)}$ = -0.016±0.045, R^2 = 0.06; $Slope_{(<20\ \mu m)}$ = 0.0081±0.013, R^2 =0.15
191 (10-Jul, 2022)	$Slope_{(>20\ \mu m)}$ = 0.044±0.044, R^2 = 0.51; $Slope_{(<20\ \mu m)}$ = 0.0080±0.022, R^2 = 0.11
198 (17-Jul, 2022)	$Slope_{(>20\ \mu m)}$ = -0.0075±0.0089, R^2 = 0.26; $Slope_{(<20\ \mu m)}$ = -0.11±0.038*, R^2 = 0.80
230 (18-Aug, 2022)	$Slope_{(>20\ \mu m)}$ = -0.14±0.048*, R^2 = 0.78; $Slope_{(<20\ \mu m)}$ = -0.079±0.028*, R^2 = 0.80
240 (28-Aug, 2022)	$Slope_{(>20\ \mu m)}$ = -0.018±0.027, R^2 = 0.18; $Slope_{(<20\ \mu m)}$ = -0.054±0.017*, R^2 = 0.83
251 (8-Sep, 2022)	$Slope_{(>20\ \mu m)}$ = -0.079±0.033*, R^2 = 0.75; $Slope_{(<20\ \mu m)}$ = -0.033±0.0053*, R^2 = 0.95
273 (30-Sep, 2022)	$Slope_{(>20\ \mu m)}$ = -0.091±0.0048*, R^2 = 0.64; $Slope_{(<20\ \mu m)}$ = -0.040±0.023*, R^2 = 0.61
280 (7-Oct, 2022)	$Slope_{(>20\ \mu m)}$ = -0.032±0.0083*, R^2 = 0.89; $Slope_{(<20\ \mu m)}$ = -0.0007±0.0061, R^2 = 0.006
296 (23-Oct, 2022)	$Slope_{(>20\ \mu m)}$ = 0.022±0.0056*, R^2 = 0.89; $Slope_{(<20\ \mu m)}$ = -0.017±0.020, R^2 = 0.25
309 (5-Nov, 2022)	$Slope_{(>20\ \mu m)}$ = 0.034±0.021*, R^2 = 0.56; $Slope_{(<20\ \mu m)}$ = 0.0061±0.0058, R^2 = 0.36
330 (26-Nov, 2022)	$Slope_{(>20\ \mu m)}$ = 0.014±0.021, R^2 = 0.19; $Slope_{(<20\ \mu m)}$ = 0.0080±0.013, R^2 = 0.15
338 (4-Dec, 2022)	$Slope_{(>20\ \mu m)}$ = 0.028±0.026, R^2 = 0.36; $Slope_{(<20\ \mu m)}$ = 0.015±0.013, R^2 = 0.38
365 (31-Dec, 2022)	$Slope_{(>20\ \mu m)}$ = 0.0075±0.0036*, R^2 = 0.68; $Slope_{(<20\ \mu m)}$ = 0.0043±0.0071, R^2 = 0.16
15 (15-Jan, 2023)	$Slope_{(>20\ \mu m)}$ = 0.026±0.0055*, R^2 = 0.92; $Slope_{(<20\ \mu m)}$ = 0.028±0.0048*, R^2 = 0.95
36 (5-Feb, 2023)	$Slope_{(>20\ \mu m)}$ = 0.027±0.0025**, R^2 = 0.98; $Slope_{(<20\ \mu m)}$ = 0.0025±0.0054, R^2 = 0.097
50 (19-Feb, 2023)	$Slope_{(>20\ \mu m)}$ = 0.038±0.0034**, R^2 = 0.98; $Slope_{(<20\ \mu m)}$ = 0.027±0.0043*, R^2 = 0.95
63 (4-Mar, 2023)	$Slope_{(>20\ \mu m)}$ = 0.048±0.023*, R^2 = 0.69; $Slope_{(<20\ \mu m)}$ = 0.038±0.013*, R^2 = 0.80
85 (26-Mar, 2023)	$Slope_{(>20\ \mu m)}$ = 0.046±0.016*, R^2 = 0.80; $Slope_{(<20\ \mu m)}$ = 0.041±0.0097*, R^2 = 0.90
106 (16-Apr, 2023)	$Slope_{(>20\ \mu m)}$ = 0.014±0.0072*, R^2 = 0.65; $Slope_{(<20\ \mu m)}$ = 0.011±0.010, R^2 = 0.38
120 (30-Apr, 2023)	$Slope_{(>20\ \mu m)}$ = 0.0047±0.012, R^2 = 0.072; $Slope_{(<20\ \mu m)}$ = 0.010±0.0025*, R^2 = 0.89
134 (14-May, 2023)	$Slope_{(>20\ \mu m)}$ = -0.0072±0.010, R^2 = 0.19; $Slope_{(<20\ \mu m)}$ = -0.017±0.0045*, R^2 = 0.88
148 (26-May, 2023)	$Slope_{(>20\ \mu m)}$ = -0.0029±0.047, R^2 = 0.001; $Slope_{(<20\ \mu m)}$ = -0.011±0.014, R^2 = 0.24
169 (18-Jun, 2023)	$Slope_{(>20\ \mu m)}$ = -0.072±0.021*, R^2 = 0.86; $Slope_{(<20\ \mu m)}$ = -0.061±0.031*, R^2 = 0.66
199 (18-Jul, 2023)	$Slope_{(>20\ \mu m)}$ = -0.093±0.023*, R^2 = 0.89; $Slope_{(<20\ \mu m)}$ = -0.080±0.0039***, R^2 = 0.99
211 (30-Jul, 2023)	$Slope_{(>20\ \mu m)}$ = -0.0052±0.021, R^2 = 0.029; $Slope_{(<20\ \mu m)}$ = -0.053±0.026*, R^2 = 0.51

Table S3. The analysis of covariance (ANCOVA). The independent variable is ambient temperature, the dependent variable is temperature sensitivity ($Slope_{F_V/F_M}$ and $Slope_{\mu}$), and the covariance is the nutrient concentrations.

Temperature sensitivity	F	*p*
$Slope_{F_V/F_M}$	>20 μm: 39.086; <20 μm: 33.741	>20 μm: <0.001; <20 μm:<0.001
$Slope_{\mu}$	>20 μm: 9.241; <20 μm: 10.807	>20 μm: <0.001; <20 μm: <0.001